A Model of Metal-Silicate Separation on Growing Planets

J. Monteux[a], Y. Ricard[a], N. Coltice[a], F. Dubuffet[a], and M. Ulvrova[a]

[a] *Université de Lyon, Lyon, F-69003, France ; Université Lyon 1, Lyon, F-69003, France ; Ecole Normale Supérieure de Lyon, Lyon, F-69364, France ; CNRS, UMR5570, Laboratoire de Sciences de la Terre, Villeurbanne, F-69622, France.*

Abstract

The thermal evolution of planets during their accretionary growth is strongly influenced by impact heating. The temperature increase following a collision takes place mostly below the impact location in a volume a few times larger than that of the impactor. Impact heating depends essentially on the radius of the impacted planet. When this radius exceeds $\sim$ 1000 km, the metal phase melts and forms a shallow and dense pool that penetrates the deep mantle as a diapir. To study the evolution of a metal diapir we propose a model of thermo-chemical readjustment that we compare to numerical simulations in axisymmetric spherical geometry and with variable viscosity. We show that the metallic phase sinks with a velocity of order of a Stokes velocity. The thermal energy released by the segregation of metal is smaller but comparable to the thermal energy buried during the impact. However as the latter is distributed in a large undifferentiated volume and the former potentially liberated into a much smaller volume (the diapir and its close surroundings) a significant heating of the metal can occur raising its temperature excess by at most a factor 2 or 3. When the viscosity of the hot differentiated material decreases, the proportion of thermal energy transferred to the undifferentiated material increases and a protocore is formed at a temperature close to that of the impact zone.

Key words: core formation; meteoritical impacts; early earth; numerical modeling; differentiation.

1. Introduction

Core formation is the most important differentiation event that occured during Earth's history. Metal/silicates separation is a rapid event (< 60 My) (Yin et al., 2002; Kleine et al., 2002; Touboul et al., 2007) contemporaneous with Earth accretion and involving gravitational mechanisms such as percolation, negative diapirism and Rayleigh-Taylor instabilities (Stevenson, 1990; Honda et al., 1993). In the homogeneous accretion hypothesis, metal segregation and thereby core formation need significant heating to exceed the melting temperature of iron alloys or of silicates. During the early stages of planetesimals formation, heating by decay of short lived radionuclides is a potential energy source to enhance early differentiation (Yoshino et al., 2003). As a planetesimal grows, its gravity increases and it will increasingly attract the other surrounding planetesimals. The dissipation of the kinetic energy of the impacts provides a later shallow source of heat.

Impacts of large planetesimals have strongly influenced the late accretionary and thermal state of nearly fully-formed planetary bodies (Tonks and Melosh, 1992; Senshu et al., 2002). During an impact, when the relative velocity between a planet and an impactor overcomes the seismic velocities of the medium, a shock wave develops. The shock pressure is nearly uniform in a spherical region next to the impact (the isobaric core), and strongly decays away from it (Croft, 1982; Pierazzo et al., 1997). In this isobaric core, the kinetic energy of the impact is dissipated and leaves a temperature anomaly of several hundred degrees on Moon to Mars size bodies (Senshu et al., 2002; Monteux et al., 2007). The temperatures reached are mostly related to the properties (density and radius) of the impacted body, and only weakly to those of the impactor (Monteux et al., 2007). The melting temperature of iron alloys is lower than the silicates solidus (Fei et al., 1997; Agee, 1997; Ghosh and McSween, 1998). On large impacted

planets, a local differentiation may occur between heavy metal and light silicates in the heated anomaly (Tonks and Melosh, 1992). Hence, a thermo-chemical readjustment follows, associated with the sinking of the metallic component toward the center of the impacted protoplanet (Fig. 1).

For large planets, gravitational energy release due to core formation can induce melting of the whole planet (Stevenson, 1989; Ricard et al., 2009). This subsequent melting depends on the mechanisms of the metal descent (Samuel and Tackley, 2008; Golabek et al., 2008). The aim of this study is to determine the thermal evolution of metal during descent and the thermal state of the core.

First, we propose analytical and numerical isoviscous models of segregation of a purely spherical iron diapir. As the viscosity contrast between molten metal and undifferentiated cold material can reach several orders of magnitude, we then focus on more realistic models of segregation of metal after a large impact with temperature dependent rheologies. We show that the size of impactors and viscosities involved largely determine the inner thermal state of a young planet.

2. Thermo-chemical state after large impact

2.1. Thermal state

After a meteoritical impact, heating is localized in a spherical region called the isobaric core just beneath the impact site. The radius of the isobaric core R_{ic} is comparable to the radius of the impactor R_{imp} and depends on energy conversion during the shock. With a minimal set of assumptions, we get $R_{ic} = 3^{1/3}\ R_{imp}$ following Senshu et al. (2002) and Pierazzo et al. (1997). Just after the adiabatic pressure release, the isobaric core is isothermal and we call ΔT_0 the shock induced temperature increase. The lower script 0 indicates that we consider this instant as the origin of our time variable. Outside the isobaric core, the temperature anomaly decays as $\Delta T_0(r) = \Delta T_0 \left(R_{ic}/r\right)^m$ with $m \sim 4.4$

as proposed by Senshu et al. (2002). Assuming that the kinetic energy of the impactor is controlled by the escape velocity of the impacted body and that impactor and impacted body have the same densities (i.e., $\rho_{ic} = \rho_{imp} \equiv \rho_0$), a simple energy balance (see e.g., Monteux et al., 2007), indicates that

$$\Delta T_0 = \frac{4\pi}{9} \frac{\gamma}{h(m)} \frac{\rho_0^2 G R^2}{\overline{\rho C_p}}, \tag{1}$$

where $\overline{\rho C_p}$ is the average heat capacity of the impacted body that is plausibly a mixture of silicate and metal, G is the gravitational constant, ρ_0 is the density of the undifferentiated material, R is the radius of the impacted planet and where the function $h(m)$ represents the volume effectively heated normalized by the volume of the isobaric core (typically $h(m) \sim 2 - 3$ (Monteux et al., 2007)). The empirical coefficient γ is the fraction of the kinetic energy of the impactor dissipated as heat. From shock experiments, γ ranges between 0.2 and 0.4 depending on material properties and shock velocities (O'Keefe and Ahrens, 1977) (i.e., 20 to 40% of the kinetic energy is buried at depth, the rest rapidly radiated away during or shortly after the impact). The shock-induced temperature excess, ΔT_0, strongly increases with the radius of the impacted body. According to the set of parameters of Table 1, $\Delta T_0(\mathrm{K}) = 4.7 \times 10^{-5} R^2(\mathrm{km})$; for a Moon size body ΔT_0 is 140 K while it is 1925 K for an Earth size body.

The thermal state of a protoplanet before an impact depends on its growth history and on its initial heating caused by short lived radionuclides like ^{26}Al and ^{60}Fe. This early radioactive heating can eventualy cause melting and differentiation of planetesimals that have quickly grown (Yoshino et al., 2003). The impact heating superimposed to a sufficiently hot protoplanetary interior can trigger melting of the Fe-FeS system (the eutectic temperature is close to 1250 K at 1 bar) (Fei et al., 1997) and potentially of silicates (solidus temperature is around 1500 K at 1 bar) (Agee, 1997). In these cases, a fraction of the thermal

energy is converted to latent heat during the phase transformations.

2.2. Compositional state

An impact on a large enough undifferentiated protoplanet composed of a mixture of metals and silicates can trigger phase transformations and initiate differentiation. The first component that melts is the metal phase. In the region where metal melting occurs, the liquid metal can percolate through the solid silicate matrix. Percolation is only possible for small dihedral angles ($< 60°$) or for large melt volume fraction above a percolation threshold. The dihedral angle of liquid iron alloy within silicates is large ($\sim 100°$) in the upper mantle but decreases with increasing pressure (Shannon and Agee, 1996). However, the volume fraction of liquid alloy is typically larger than 10% if melting is complete, which overcomes the percolation threshold (Von Bargen and Waff, 1986). On Earth the core represents 17% of the volume of the planet, Mars has likely a slightly smaller core but Mercury's core is 43% of the planet. The metal is collected at the bottom boundary of the melted zone forming a diapir that ultimately sinks within the interior of the impacted protoplanet (Ricard et al., 2009).

If the temperature exceeds the silicate solidus and eventually the liquidus, the separation of metal and silicates can occur as a metal rainfall through a turbulent magma (Stevenson, 1990; Höink et al., 2005). Small droplets of heavy metal sediment at the bottom of the melted region. This scenario may not be the generic one, as it would imply that a planet embryo maintains a melted metal component without differentiating until the silicates start melting. It has been suggested that the metal may segregate per percolation, as soon as it melts, while the silicates are still mostly solid (Ricard et al., 2009). Locally, however, the impact of an undifferentiated planetesimal on an already differentiated large planetary embryo, may of course, be energetic enough to melt (or even vaporize)

the silicate and metal contents of the impactor and the silicates of the impacted body inside the isobaric core.

The two processes (percolation or metal "rain") lead to a local differentiation within the melted region between light silicates and heavy metals on a short timescale compared to that of the slow viscous deformation (Tonks and Melosh, 1992). The melted region is as large as or a few times larger than the isobaric core (Pierazzo et al., 1997). Here, we identify the initially differentiated zone to the isobaric core, metal being overlaid by pure silicates shortly after the impact (see Fig.1).

3. Dynamic model of differentiation

The setting described in the previous section is gravitationally unstable and the metal phase sinks toward the center of the impacted planetesimal while the silicates (lighter than undifferentiated material) spread underneath the surface. To study the global dynamics of this differentiation event, we develop a thermo-mechanical model in spherical axisymmetrical geometry, of viscous flow with three chemical components. Using a viscous and linear rheology during the segregation of the core is clearly a large approximation. The large deviatoric stress generated by the metallic diapirs should lead to a non-linear rheology (Samuel and Tackley, 2008), elasto-plastic deformations (Gerya and Yuen, 2007) or even to hydrofracturation if they exceed the ultimate strength of rocks which is $\sim 1-2$ GPa (Davies, 1982). Pressure dependence of the rheology can also influence the metal sinking time but is not considered here since we focus on small growing planets. During the early stages of accretion, the interior of the growing planets may have been colder or hotter than the outer layers depending on the ratio of radioactive and impact heating and on the history of accretion. For simplicity, we assume in our models an homogenous temperature on the

158 growing planet before the impact.

159 *3.1. Physical model*

160 Sinking occurs under the action of gravity in a spherical homogeneous pro-
161 toplanetary body. We neglect for simplicity the changes of gravity during the
162 differentiation. Hence gravitational acceleration $g(r)$ increases linearly with ra-
163 dius r:

$$g(r) = \frac{4}{3} G\pi\rho_0 r = g_0 \frac{r}{R}, \tag{2}$$

164 where g_0 the surface gravity. The density of undifferentiated material is $\rho_0 =$
165 $f_0\rho_{Fe} + (1 - f_0)\rho_{Si}$ where f_0 is the volume fraction of metal and ρ_{Fe}, ρ_{Si}, the
166 densities of the metallic phase and the pure silicates, respectively (see typical
167 numerical values in Table 1.)

168 The dynamics of segregation potentially involves a series of multiscale physi-
169 cal processes, especially to take the effects of melting into account and a realistic
170 multiphase dynamics (Golabek et al., 2008; Ricard et al., 2009). No numerical
171 models can handle simultaneously all these complexities and as a consequence,
172 we follow the approach of Samuel and Tackley (2008) and consider a thermo-
173 chemical system with infinite Prandtl limit, with no possible subsequent phase
174 separation within the undifferentiated material except that caused by the im-
175 pact (e.g., the volumes of pure metal and pure silicates remain constant during
176 the simulations and equal to 17% and 83% of the initial isobaric core).

177 The necessary approximations are somewhat different from the classic treat-
178 ment of thermal convection (see e.g., Ricard, 2007). We non-dimensionalize the
179 lengths by the planetary radius R, the velocities by a Stokes velocity $\Delta\rho_0 g_0 R^2/\eta_0$
180 (where $\Delta\rho_0 = \rho_{Fe} - \rho_{Si}$ and η_0 is the reference viscosity of cold material far from
181 the impact site), the temperature by ΔT_0 (see Eq.1). The governing mechanical
182 non-dimensionnal equations are the conservation of mass

$$\boldsymbol{\nabla} \cdot \mathbf{v} = 0, \tag{3}$$

and the conservation of momentum

$$-\boldsymbol{\nabla} P + \boldsymbol{\nabla} \cdot \left(\frac{\eta}{\eta_0} \left[\boldsymbol{\nabla} \mathbf{v} + [\boldsymbol{\nabla} \mathbf{v}]^T \right] \right) + \left(\frac{T}{B} - f \right) r \mathbf{e_r} = 0, \tag{4}$$

where $\mathbf{v}$, P, T and r are the non-dimensional velocity, pressure, temperature and radius, η the viscosity, T_0 the temperature (assumed uniform) before the impact and $\mathbf{e_r}$ the radial unit vector. The buoyancy ratio B (Christensen and Yuen, 1985) is:

$$B = \frac{\Delta \rho_0}{\rho_0 \alpha \Delta T_0}. \tag{5}$$

The downward buoyancy force that drives the flow increases with the volume fraction of metal f that varies between 0 (pure silicates) and 1 (pure metal), 0.17 being that of undifferentiated material. A depth dependent and constant in time gravity has been used in the momentum equation Eq.4 although, in principle, gravity should have been computed self-consistently from the time-dependent density distribution. We assume a temperature dependent viscosity such as $\eta = \eta_0 \lambda^T$ with λ being the viscosity factor (lower than 1) which is equivalent to the viscosity ratio between the hottest and coldest material at the start of the experiment. Such a viscosity decreases sharply with temperature and is simpler to implement than the usual Arrhenius law (Ratcliff et al., 1997; Ziethe and Spohn, 2007).

The conservation of energy writes

$$\frac{DT}{Dt} = \frac{\nabla^2 T}{Ra_\chi} + D_\chi \frac{\eta}{\eta_0} \Phi + \frac{1}{B} \frac{\Delta \rho}{\rho} \frac{T}{\Delta T_0} D_\chi \frac{DP}{Dt}. \tag{6}$$

The importance of diffusion is controlled by the compositional Rayleigh num-

ber Ra_χ,

$$Ra_\chi = \frac{\Delta\rho_0 g_0 R^3}{\kappa\eta_0}, \tag{7}$$

the chemical dissipation number is

$$D_\chi = \frac{\Delta\rho_0 g_0 R}{\overline{\rho C_p}\Delta T_0}, \tag{8}$$

considering for simplicity that $\overline{\rho C_p} = \rho_{Fe} C_p^{Fe} = \rho_{Si} C_p^{Si}$ (truely, see Table 1, $\rho_{Fe} C_p^{Fe} = 4 \times 10^3$ kJ K^{-1} m^{-3}, $\rho_{Si} C_p^{Si} = 3.85 \times 10^3$ kJ K^{-1} m^{-3}, and we use $\overline{\rho C_p} = 4 \times 10^3$ kJ K^{-1} m^{-3}). As g_0 is proportional to R and ΔT_0 to R^2, see Eq.1, the chemical dissipation is independent of the planet radius and amounts to 36.6 (see Table 1).

An important energy source is provided by the dimensionless dissipation function Φ that expresses the conversion of potential energy into heat

$$\Phi = 2\,\underline{\boldsymbol{\epsilon}} : \underline{\boldsymbol{\epsilon}}. \tag{9}$$

where $\underline{\boldsymbol{\epsilon}}$ is the dimensionless strain rate tensor. For simplicity, we make the approximation that the thermal conductivities of the metal, silicates and undifferentiated materials are the same (truely k_{Fe}=10 W m^{-1} K^{-1}>k_{Si}=3 W m^{-1} K^{-1}).

The metal volume fraction is then simply advected by the flow,

$$\frac{Df}{Dt} = 0. \tag{10}$$

3.2. Model approximations

The equations of momentum and energy conservations, Eq.4 and Eq.6, are similar to those classically used for mantle convection simulation but a number of differences should be discussed. As the buoyancy number B is very large (the

density difference between metal and silicates is 40 to 620 times larger than the thermal density variations), the thermal buoyancy T/B can be safely neglected in the momemtum equation.

Neglecting the terms in $1/B$ implies to omit the adiabatic heat transfer (the term in (DP/Dt)) in Eq.6 but to keep the dissipation term $D_\chi(\eta/\eta_0)\Phi$. The differentiation of the planet liberates a large amount of potential energy converted into heat by the dissipation term but the adiabatic heating remains small. This is very different from the typical convection situation in which there is no time variation of the potential energy, and where the dissipation is on average, balanced by the work due to compression and expansion over the convective cycle (Hewitt et al., 1975).

3.3. Numerical model

We implement a finite volume numerical model to solve Eq.3, Eq.4, Eq.6 and Eq.10 in axi-symmetric spherical geometry. We use a stream function formulation for the equations of motion with a direct implicit inversion method (Schubert et al., 2001). Eq.6 and Eq.10 are solved by an Alternating Direction Implicit (ADI) scheme (Peaceman and Rachford, 1955; Douglas, 1955). The stream function, temperature and compositional fields are described by a second-order approximation in space. To limit numerical diffusion when solving the transport equations, especially for the compositional field, we use a Total Variation Diminishing Superbee scheme (Roe, 1986; Laney, 1998) implemented in an implicit way (Sramek, 2007) which enables a high resolution of pure advective fields. We use at least 200×200 grid points. Velocity boundary conditions are free-slip at the surface and along the symmetry axis. Thermal boundary conditions are isothermal at the surface and insulating along the symmetry axis. We benchmark the viscous flow solver with variable viscosity and the transport scheme against several analytical solutions (Monteux, 2009).

4. Thermal evolution of sinking metallic diapir: Analytical considerations

Before showing the results of complex numerical simulations with temperature dependent rheologies, we develop a simple model describing the thermal evolution of the sinking metal diapir, by approximating the metal diapir by a spherical drop falling into undifferentiated medium of uniform viscosity with a Stokes-like velocity. The radius of the metal drop R_{Fe}, can be related to the radius R_{ic} of the volume initially differentiated after impact heating, by $R_{Fe}^3 = f_0 R_{ic}^3$ and to the radius of the impactor by $R_{Fe}^3 = 3 f_0 R_{imp}^3$.

4.1. Sinking velocity

The velocity V of the metallic diapir in an undifferentiated medium is comparable to the Stokes velocity of a sphere of similar volume. The density difference between the metal and the undifferentiated material is a function of temperature and composition but the temperature contribution is minor. Hence, we consider $\Delta\rho = (1 - f_0)\Delta\rho_0$. Because gravity is a linear function of depth, the velocity of the sphere decreases during sinking as

$$V = \frac{dr}{dt} = -c_1(1 - f_0)\frac{\Delta\rho_0 g_0 R_{Fe}^2}{\eta_S}\frac{r}{R}. \tag{11}$$

In equation Eq.11, the dimensionless constant c_1 depends on the geometry of the system and on the viscosity contrast between the falling sphere and the surrounding medium.

The viscosity of the surrounding undifferentiated material η_S controls the sinking velocity. In the case of a sphere sinking in an infinite medium, the coefficient c_1 is given by the Hadamard-Rybczynski equation and varies from $4/15 = 0.27$ (isoviscous) to $1/3 = 0.33$ for an inviscid sphere (Hadamard, 1911; Rybczynski, 1911). In the situation described in this paper, the boundary condi-

tions are applied at a finite distance (the planetary surface) and the Hadamard and Rybczynski equation is thus only an approximation (Honda et al., 1993; Samuel and Tackley, 2008). The exact value of the constant c_1 will be obtained later through numerical experiments.

The position of the metallic drop obtained by solving Eq.11 varies from an initial position r_0 ($r_0 = R - R_{Fe} \sim R$) as

$$r(t) = r_0 \exp(-\frac{t}{\tau_S}), \tag{12}$$

with a characteristic time equal to

$$\tau_S = \frac{\eta_S R}{c_1 \Delta\rho_0 g_0} \frac{1}{(1-f_0)} \frac{1}{R_{Fe}^2}. \tag{13}$$

As g_0 is proportional to the planetary radius R (Eq.2), the time τ_S is independent of the planetary radius but depends only on the diapir size R_{Fe}. Of course, no segregation occurs, i.e., $\tau_S \rightarrow +\infty$, for a planet of pure silicates ($f_0 = 0$ which means $R_{Fe} = 0$) or of pure metal ($f_0 = 1$). This characteristic sinking time is strongly dependent of the viscosity of the surrounding undifferentiated material which is poorly constrained. With the typical values of Table 1, this time can be computed from the size R_{imp} of the impactor and we find $\tau_S(\text{kyr}) = 2.7 \times 10^9 (\eta_S/\eta_0) R_{imp}^{-2}(\text{km})$.

4.2. Global energy conversion

As we assume that gravity remains constant with time (albeit non-uniform), the energy equation Eq.6 integrated over the whole planet with the use of the momentum equation Eq.4 and neglecting the adiabatic decompression of the planet during the core segregation is simply

$$\frac{d}{dt}(\Delta E_p + \Delta E_T) = F, \tag{14}$$

where the total potential and thermal energies changes are

$$\Delta E_p = \int_\Omega \frac{1}{2} \left[\rho(\mathbf{r},t) - \rho(\mathbf{r},0)\right] g_0 \frac{r^2}{R}\, dV, \tag{15}$$

(Ω is the planetary volume),

$$\Delta E_T = \int_\Omega \overline{\rho C_p} \left[T(\mathbf{r},t) - T(\mathbf{r},0)\right]\, dV, \tag{16}$$

and the heat flux F is ,

$$F = \int_\Sigma k \frac{\partial T}{\partial r}\, dS, \tag{17}$$

(Σ is the planetary surface).

As we neglect the term in $1/B$ in the energy equation Eq.4, the budget Eq.14 misses the energy variation ΔE_a due to the changes in pressure (the subscript a means that this term is related to changes in adiabatic compression)

$$\frac{d\Delta E_a}{dt} = \int_\Omega \alpha T \frac{\partial P}{\partial t}\, dV \sim \alpha T_0 \frac{d}{dt} \int_\Omega \left[P(\mathbf{r},t) - P(\mathbf{r},0)\right]\, dV \tag{18}$$

(where the last approximation assumes that the temperature remains close to T_0). The difference of pressure between a homogeneous and a differentiated planet is easy to compute analytically and is of order $\alpha T_0 \Delta E_p$, i.e., a few percent of the changes in potential energy. This confirms that the energy change due to pressure changes is a minor effect.

4.3. Maximum temperature

The maximum temperature that the sinking metal can reach can be estimated by assuming that the whole variation of potential energy is only used to heat up the metal, without any heat transfer to the surrounding material.

Let us consider a melted zone of radius R_{ic} underneath and tangent to the planetary surface that differentiates ultimately forming a metallic core of volume V_{Fe} and radius R_{Fe} (with $R_{Fe}^3 = f_0 R_{ic}^3$) and a silicate layer of volume V_{Si} within a shell surrounding the whole planet with inner shell radius R_S and outer shell radius R i.e., $R_S^3 = R^3 - (1-f_0)R_{ic}^3$. The change of potential energy is according to Eq.15 (see also Flasar and Birch, 1973):

$$\Delta E_p = \frac{2\pi}{5R} g_0 \left((\rho_{Fe} - \rho_0) R_{Fe}^5 + (\rho_{Si} - \rho_0)(R^5 - R_S^5) \right). \tag{19}$$

Assuming $R_{ic} << R$, a Taylor expansion of Eq.19 leads to

$$\Delta E_p \sim -\frac{1}{2}\Delta\rho_0 g_0 R f_0 (1-f_0) V_{ic} = -\frac{1}{2}(\rho_{Fe} - \rho_0) g_0 R V_{Fe} = -\frac{1}{2}(\rho_0 - \rho_{Si}) g_0 R V_{Si}, \tag{20}$$

where V_{ic} is the volume of the isobaric core. The change of potential energy is thus equivalent to that released by the sinking of the isobaric volume V_{ic} and excess density $f_0(1-f_0)\Delta\rho_0$. Alternatively it corresponds to the energy released by a metal sphere of volume V_{Fe} sinking, or of a silicate sphere rising, through undifferentiated material. If only the metal heats up, the change of thermal energy according to Eq.16 is $\Delta E_T = \overline{\rho C_p} f_0 \Delta\Theta V_{ic}$ where $\Delta\Theta$ is the temperature increase (just after the impact, the metal temperature is $T_0 + \Delta T_0$, then it reaches at most $T_0 + \Delta T_0 + \Delta\Theta$). A scaling value for the temperature increase during segregation is thus

$$\Delta\Theta = \frac{1-f_0}{2} \frac{1}{\overline{\rho C_p}} \Delta\rho_0 g_0 R. \tag{21}$$

As g_0 is proportional to R (Eq.2), the core segregation can increase the temperature by a quantity proportional to R^2 (in agreement with Flasar and Birch, 1973; Ricard et al., 2009). The ratio of $\Delta\Theta$ to the post impact temperature

ΔT_0 is, according to Table 1 and Eq.1,

$$\frac{\Delta\Theta}{\Delta T_0} = \frac{3h(m)}{2\gamma}(1-f_0)\frac{\Delta\rho_0}{\rho_0} \sim 11.8 \tag{22}$$

or, $\Delta\Theta(\mathrm{K}) = 11.8\ \Delta T_0(\mathrm{K}) = 5.6\times10^{-4}R^2(\mathrm{km})$ which rapidly becomes a large quantity as R increases. Of course, in a real situation not all energy will remain within the metal, and we will see that, when the metal diapir is too small, the metal can even cool off rather than warm up during its motion.

4.4. Thermal regime of the metallic sphere

While the hot metallic sphere is sinking, it warms up by shear heating but it also cools down by diffusion. In the reference frame of the sinking drop, the conservation of energy integrated over the volume V_{Fe} of the metallic drop (or through its surface S_{Fe}) indicates that

$$\overline{\rho C_p} V_{Fe}\frac{d\Delta T}{dt} = -k\frac{\Delta T}{\delta}S_{Fe} + \underline{\boldsymbol{\tau}} : \boldsymbol{\nabla}\mathbf{v}\ V_{Fe}, \tag{23}$$

where we assume that the temperature and the dissipation are at first order uniform in the metal. The difference ΔT is the difference between the diapir and the undifferentiated material. We assume that $\Delta T = T - T_0$, i.e., that the hot diapir sinks into a medium that keeps its initial temperature outside the boundary thickness δ. Even when the diapir viscosity is low and when the dissipation occurs significantly outside it, our numerical simulations shows that the maximum temperature is reached inside the diapir.

The thickness δ over which the temperature diffuses should be written as R_{Fe} times a dimensionless function c_2 of the various parameters of the problem. The thickness of the diffusive boundary layer, c_2, should decrease with the sinking velocity of the diapir (i.e., with the Peclet number VR_{Fe}/κ) as a power law with exponent -1/2 or -1/3, depending on the viscosity ratio between the metal

and the undifferentiated material (see e.g., Ribe, 2007). We can also write the dissipation $\underline{\boldsymbol{\tau}} : \boldsymbol{\nabla}\mathbf{v} = \eta_e V^2/R_{Fe}^2$ where η_e is the effective viscosity of the region where dissipation occurs. In this case, Eq.23 using the expressions of the time dependent position, Eq.12, and of the maximum temperature increase, Eq.21, can be recast as

$$\frac{d\Delta T}{dt} = -\frac{\Delta T}{\tau_D} + 2a\left(\frac{r_0}{R}\right)^2 \frac{\Delta\Theta}{\tau_S} \exp\left(-2\frac{t}{\tau_S}\right), \tag{24}$$

where the dimensionless constant

$$a = c_1 \frac{\eta_e}{\eta_S} \tag{25}$$

characterizes the proportion of heat effectively dissipated in the metal and τ_D the characteristic time of diffusion

$$\tau_D = \frac{c_2 R_{Fe}^2}{3\kappa}, \tag{26}$$

where c_2, measuring in terms of R_{Fe} the thickness of the thermal boundary layer around the metal, $\delta = c_2 R_{Fe}$, is a dimensionless number.

Eq.24 cannot be used predictively in a complex situation as it requires the knowledge of various parameters c_1, c_2 and a. The dependences of these parameters with more fundamental quantities (mostly with the temperature dependence of the viscosity) have to be determined empirically. We will see however, that for a given choice of the rheology, Eq.24 captures the evolution of the metallic diapir temperature as a function of time and the dependence of this temperature with the diapir size. For example, Eq.24 suggests that the diffusion term decreases with R_{Fe} (as R_{Fe}^{-2} if one considers c_2 as a constant) while the dissipation term increases with R_{Fe}^2. We can also use Eq.24 qualitatively by

assuming $a \sim c_1 \sim 4/15$ (using Stokes law) and $c_2 \sim 1$.

The expression Eq.24 shows that the temperature is not necessarily an increasing function of time. More precisely, according to Eq.24 the metal temperature increases just after the impact ($t \sim 0$), if

$$-\frac{\Delta T_0}{\tau_D} + 2a\left(\frac{r_0}{R}\right)^2 \frac{\Delta\Theta}{\tau_S} > 0 \tag{27}$$

Using the expressions for the temperature increase upon impact ΔT_0 (see Eq.1), the maximum temperature increase during segregation $\Delta\Theta$ (see Eq.21) and for the two time constant τ_S and τ_D (see Eq.13 and Eq.26), this condition implies that dissipative heating overcomes the conductive diffusion when

$$R_{Fe} > R_{Fe,min} \tag{28}$$

where $R_{Fe,min}$ involves the properties of the planet, but not its radius since ΔT_0 is proportional to R^2:

$$R^4_{Fe,min} = \frac{9}{8\pi}\left(\frac{r_0}{R}\right)^2 \frac{1}{c_1 c_2 a}\frac{\Delta T_0}{\Delta\Theta}\frac{\eta_S \kappa}{G\rho_0(1-f_0)\Delta\rho_0}. \tag{29}$$

According to the set of parameters shown in Table 1, $R_{Fe,min} \sim 45$ km (using $c_1 \sim a \sim 4/15$, $r_0 \sim R$ and $c_2 \sim 1$ but using values fitted from experiments does not change this radius very much for the moderate level of viscosity variations used in our simulations herafter). Such a diapir corresponds to an impactor of radius $R_{imp} \sim 60$ km ($R_{imp} = R_{ic}/3^{1/3} = R_{Fe}/(3f_0)^{1/3}$). Therefore, only impactors larger than $R_{imp} = 60$ km generate metallic diapirs that heat up during sinking, although their initial temperature set by the impact is not dependent on the size of the impactor.

Integration of Eq.24 leads to:

$$\Delta T = \Delta T_0 \exp(-\frac{t}{\tau_D}) + a\left(\frac{r_0}{R}\right)^2 \Delta\Theta \frac{2\tau_D}{2\tau_D - \tau_S}\left(\exp(-\frac{t}{\tau_D}) - \exp(-2\frac{t}{\tau_S})\right). \quad (30)$$

The initial temperature anomaly ΔT_0 decreases exponentially with time while the interplay between diffusion and dissipation controls the general temperature evolution. For the diapir to heat up, the heating time $\tau_S/2$ must be shorter than the diffusive time τ_D. Typically $r_0 \sim R$ and in the regime where the diapir heats up, the dissipation occurs before the diffusion, $\tau_S/2 << t << \tau_D$; the temperature rapidly increases to $\Delta T = \Delta T_0 + a\,(r_0/R)^2\,\Delta\Theta$, and the physical interpretation of a is therefore the percentage of heat dissipated inside the metal. According to Eq.25, a should be lower than the coefficient c_1 of the Rybczinski-Hadamard velocity as the effective viscosity of the hot diapir η_e is likely lower than the average viscosity η_S. For a numerical application we take however $a \sim c_1 = 4/15 \sim 0.27$ as obtained for the isoviscous Rybczinski-Hadamard velocity. As $\Delta\Theta$ and ΔT_0 are simultaneously proportional to R^2, the maximum temperature of the diapir is at most $\Delta T = 4.2\,\Delta T_0$ and is independent of the planet size.

Dissipation decreases as $\exp(-2t/\tau_s) = (r/r_0)^2$ according to Eq.12. Hence, the dissipation term in Eq.24 decreases with depth. When a diapir heats up, its temperature increases therefore to the maximum ΔT_{max} reached at the radius r that satisfies $d\Delta T/dt = 0$ or

$$0 = -\frac{\Delta T_{max}}{\tau_D} + 2a\frac{\Delta\Theta}{\tau_S}\left(\frac{r}{R}\right)^2, \quad (31)$$

which implies

$$\left(\frac{r}{r_0}\right)^2 = \frac{\Delta T_{max}}{\Delta T_0}\left(\frac{R_{Fe,min}}{R_{Fe}}\right)^4. \quad (32)$$

The factor $\Delta T_{max}/\Delta T_0$ varies between 1 (no heating) and 4.2 (maximum esti-

mated temperature). As an example, an impactor of radius 120 km, generates a metallic diapir of 96 km (two times $R_{Fe,min}$) that heats up until it reaches half the radius of the impacted planet. The expression Eq.32 is only valid when $R_{Fe} > R_{Fe,min}$, otherwise the diapir temperature simply decreases.

5. Numerical simulations

We compare the predictions of the analytical model to spherical axisymmetric calculations of a sinking metallic drop, especially to extract the diffusive and sinking times τ_D and τ_S and the fraction of heat trapped in the metallic phase (e.g., the constants c_1, c_2 and a, that we expect to be close to 4/15, 1 and 4/15). We then compare these results to more complex numerical experiments where a compositional anomaly is generated in the isobaric core after a large impact. The effect of variable viscosity is also studied in these models.

5.1. Numerical models of sinking metallic drops

5.1.1. Sinking velocity

We solve numerically a set of problems in which we introduce metallic spheres ($f_0 = 1$) of different sizes, tangent to the surface, in undifferentiated planets ($f_0 = 0.17$) of various radii. From this set of experiments, we compare the temporal evolution of the sphere position to what is predicted by Eq.12. The calculations presented here are isoviscous for simplicity but variable viscosity will be introduced in more complex cases. Fig.2 shows that the values of τ_S obtained by fitting the center of the diapir position to an exponential in the numerical models, vary as $1/R_{Fe}^2$ as expected from the analytical model, with $c_1 = 0.187$ (almost 70% of the Hadamard-Rybczynski velocity for a homogenous viscosity 4/15=0.27). For large sphere radii, boundary effects are stronger and the sinking times are slightly larger.

5.1.2. Temperature evolution

Large sinking diapirs heat up before cooling down by diffusion when the velocity of the metal decreases sufficiently towards the center. Our theoretical predictions given by Eq.30 are in good agreement with the computed evolutions with the value c_1 obtained previously. Fig.3 shows the consistency between the numerical results and the theory when the parameters c_2 and a are fitted ($c_2 = 0.72$, $a = 0.2$ which is reasonably close to $c_1 = 0.187$). The value of a , indicates that 20% of the released heat is trapped in the metal. The maximum temperature value, $2.2\,\Delta T_0$, is in rough agreement with the estimate $\Delta T = \Delta T_0 + a\,(r_0/R)^2\,\Delta\Theta = 2.88\,\Delta T_0$. This value is obtained for sufficiently large impactors (> 200 km) since smaller ones can cool off very early upon sinking as seen from Eq.32.

We monitor the temperature evolution for various diapir radii. Fitting the temperature evolution with Eq.30 leads to values of τ_D and a for each diapir radius. The corresponding characteristic diffusive times are plotted in Fig.4. These times are consistent with analytical predictions from Eq.26 and increase with the square of the diapir size. For all the experiments, the fraction of heat a trapped in the metal is therefore reasonably constant ($\sim 22 \pm 5\%$) and close to c_1.

To verify condition Eq.32 that predicts the radius for which dissipation overcomes diffusion, we computed the rate of heating or cooling of metallic spheres as a function of their radius and depths. Various planetary radii have been used and, as predicted, the heating always occur in the external part of the planet (filled symbols). Near the center of the impacted planet, when the gravity decreases, diffusion dominates (open symbols) and the temperature of the sinking metallic phase decreases. As shown in Fig.5, the transition between heating and cooling occurs consistently within the shaded area predicted by the analytical

457 expressions Eq.32. For small diapirs ($R_{Fe} \leq 45$ km), diffusion dominates and
458 prevents heating. Large diapirs reach their maximum temperature and start
459 cooling near the high temperature estimate of the analytical model.

460 *5.2. Application to global evolution after an impact*

461 The thermo-chemical initial conditions after an impact differ from a simple
462 hot metallic sphere sinking within an undifferentiated material. Indeed, the
463 denser metallic pond collected at the bottom of the isobaric core is not spher-
464 ical and above it, a volume of light silicates rises and spreads underneath the
465 surface until it covers the entire surface of the planet. These deviations from
466 our analytical model potentially modify the results obtained from the sinking
467 metallic drop model. Here we show numerical simulations of segregation after
468 an impact and compare them to the analytical model previously developed.

469 Fig.6 depicts the thermal and compositional evolution after an impact of
470 a large impactor ($R = 4000$ km, $R_{imp} = 600$ km and $R_{Fe} = 480$ km). The
471 four rows correspond to real time snapshots at 0, 1.4, 3.8 and 546 Myrs. The
472 temperature field is depicted in the left column, and the composition in the right
473 column (undifferentiated material in light blue, metal in red, silicates in green).
474 The metallic pond sinks towards the center of the planet while heating. This
475 heating is in agreement with our previous findings that dissipation is larger than
476 diffusion for large impacts. However, the metal develops a tail through sinking
477 and is significantly deformed. In the meantime, the light silicates rise upward
478 and heat up as well, while stretching laterally to cover the whole surface of the
479 planet. Of course, the diffusion of heat out of the silicate layer near the surface,
480 is much faster than that out of the deep protocore and this shallow hot silicate
481 layer cools rapidly. On a much longer time scale (assuming irrealistically that
482 no other impact occurs, hot thermal plumes should start from the proto core-
483 mantle boundary and deliver the protocore heat to the surface (Behounkova and

Choblet, 2009).

Fig.7 illustrates the evolution of the conversion from potential to thermal energy with time. During the thermo-chemical reequilibration, the potential energy (thick line) decreases as the metal approaches the center and as the silicates spread beneath the surface. Viscous heating induces an increase of thermal energy (grey line). Once the metal has reached the center of the impacted protoplanet, the thermal energy can only decrease. During this whole process, heat is slowly removed by diffusion through the surface of the planet and the cumulative heat flux (dotted line) balances the total energy budget. This global balance (sum of potential energy, thermal energy and cumulative heat flux (see Eq.14)) is closely satisfied which illustrates the good accuracy of the numerical code.

We now introduce a temperature-dependence of the viscosity in the calculations. Experimental results suggest that the viscosity contrast between melt iron and solid silicates can reach 20 orders of magnitude (Vocadlo et al., 2000). Such a viscosity contrast is difficult to handle numerically and we use much smaller values.

In our models, the viscosity varies as $\eta = \eta_0 \lambda^T$ and as the temperature of metal may increase while sinking by a factor up to 2, it implies maximum viscosity contrasts up to $1/\lambda^2$ orders of magnitude between cold and hot materials. Using a composition dependent viscosity would have been more realistic but viscous fronts are too difficult to handle numerically. We compare the thermo-chemical states at the same time, $t = 3.2$ Myr for different viscosity factors in Figure 8. We use $\lambda = 0.25$ (Figure 8 second row), $\lambda = 0.1$ (Figure 8 third row) and $\lambda = 2.5 \times 10^{-2}$ (Figure 8 bottom row), the top row being the reference isoviscous case.

Increasing the temperature-dependence of the viscosity softens the surround-

ing material around the metallic drop and the metallic diapir, at a given time, is closer to the center when its viscosity is decreased, as shown in Fig.8. However, this effect remains small. Because the metallic pond becomes less viscous, its shape becomes more spherical and the tail developed in isoviscous experiments becomes thinner. Increasing the sinking velocity increases the rate of shear heating but not the total release of thermal energy which is only related to the change in gravitational energy. Lowering the viscosity in the surrounding material and within the metallic pond has also the effect of diminishing η_e. The dissipation is therefore increased in the undifferentiated material and decreased in the hot and less viscous metallic diapir. This effect combined with the faster spreading of the hot silicate that removes the heat more rapidly lead to lower maximum temperatures (see Fig.8).

We monitor the position of the inertia center of the metallic diapir as a function of time and compute the sinking times τ_S (see Figure 9). The position of the diapir obeys reasonably to the exponential law predicted by Eq.12. In the isoviscous case, the observed normalized time is $\tau_S = 563$ which is twice longer than what is predicted by Eq.13. This is due to the fact that the initial diapir shape is not spherical and to the presence of the rising volume of silicates. When the viscosity decreases with temperature the sinking is faster, $\tau_S = 249$, 170 and 114, for $\lambda = 0.25$, 0.1 and 2.5×10^{-2} (see Fig.9 and Tab.2). This is due to two effects: the reduction of viscosity inside the metal (the Rybczinski-Hadamard formula predicts an increase of the velocity factor c_1 from 0.27 to 0.33 when the interior viscosity of the diapir decreases) and the decrease of viscosity of the heated surrounding material.

In the experiments depicted in Fig.6 and Fig.8, the metal temperature increases and reaches a value close to twice the initial temperature of the isobaric core (Fig.10). However, heating within the metal is less pronounced with vari-

able viscosity and decreases with the viscosity contrast. Fitting the computed temperature evolutions in the metallic diapirs with our theoretical model gives values of c_2 in the isoviscous case and the variable viscosity cases (see Tab.2 and Fig.10). The thickness of the thermal boundary measured by c_2 decreases with the sinking velocity (the Peclet number). The values of c_2 and of τ_D are therefore related to $Pe^{-n} \propto \tau_S^n$ with an exponent $\sim 1/3$ in the range of values, $n = 1/2 - 1/3$ predicted in Ribe (2007).

When the temperature dependence of the viscosity increases, the proportion of energy heating the metal diapir, a, decreases (see Tab.2). As a consequence, the heat release of the gravitational energy becomes increasingly efficient in the surrounding undifferentiated material. This suggests that a diapir of very small viscosity does not heat much during its motion while most of the release of gravitational energy occurs in the undifferentiated materials. A low viscosity diapir keeps basically its initial temperature because its characteristic diffusive time is larger than its sinking time and also because of the buffering effect of the temperature dependent viscosity (i.e., a too large cooling would increase the viscosity and would bring back the dissipation within the diapir itself).

6. Discussion and conclusion

Core formation events induced by meteoritical impacts play a major role in determining the early thermo-chemical state of growing planets. Large meteoritical impacts can trigger a local differentiation between metal and silicates in a spherical zone above the surface called the isobaric core. The segregation of dense and light phases through the undifferentiated material of the impacted protoplanet induces a large viscous heating.

We followed the dynamics of the metal phase after a large impact with numerical experiments in axisymmetrical spherical geometry. The sinking velocity

of the metal phase is Stokes-like and is function of the viscosity contrast between the metal phase and the undifferentiated crossed media. The velocity increases when viscous heating decreases the viscosity of the surrounding material. A stress dependent viscosity (not considered here) would also increase this velocity (Samuel and Tackley, 2008). The sinking process in a planet with a cold interior compared to its surface would eventually imply higher viscosity contrasts between the metal and the surrounding material and would lead to longer sinking times.

The gravitational energy release during the segregation is converted into viscous heating in the metal and in the silicates. Our results show that a net viscous heating of the metallic phase only occurs for large metallic diapirs ($R_{Fe} > 45$ km). This metallic volume at the bottom of the isobaric core would be produced by an impactor of order $R_{imp} > 60$ km. This result underlines the importance of accretion conditions on the inner thermal state of planetary bodies. Small metallic diapirs cool while sinking and may ultimately bring the metal in a solid state to the core of the impacted planet.

The heat repartition between the metal phase, the silicates and the undifferentiated material is not only a function of the size of the metallic diapir but also of the rheology of the various phases. For low viscosity of the metal and of the sheared zone around the metallic diapir, the metal phase is weakly heated. Hence, gravitational energy release will mainly lead to the heating of the surrounding undifferentiated material and ultimately to its differentiation.

The viscosity variations that we explore in our simulations are of order $\lambda^{\Delta T_{max}}$ which in the most extreme cases reach about four orders of magnitude over very short distances. This is certainly modest relative to the viscosity contrasts of 20 orders of magnitude that exists between liquid metal and solid silicates (Vocadlo et al., 2000). Viscosity contrasts based on composition rather

than temperature would be more realistic but would have occurred on even shorter distances (the computation grid itself) that could not be resolved with classical numerical methods. Our model is therefore an end-member of possible models on heating modes during core formation. However the description of the physics of the processes would still be valid for larger viscosity contrasts.

As soon as a growing planet reaches a few 1000 km in radius R, the heating by impacts becomes significant (the temperature increase varies as R^2 and reaches 400 K for $R = 3000$ km, (Monteux et al., 2007)). This temperature increase superimposed on the fossil temperature T_0 from short half-life radionucleides (^{26}Al and ^{60}Fe) and previous impacts can lead to a temperature larger than the melting temperature of the metallic phase. Our analytical models confirmed by numerical experiments show that the metallic drop reaches the planet center in a time depending on the size of the metallic drop and the background viscosity of the planet but not of its radius (see Eq.13). Even in the case where the impacted planet is relatively cold and with a high viscosity of 10^{22} Pa s, this time is smaller than a few million years for an impactor of 300 km. The sinking timescales obtained in our models are comparable to those obtained with an Arhenius rheology (Ziethe and Spohn, 2007) and within the timeframe required for an early core formation (< 60 My). The temperature increase in the undifferentiated material localized along the sinking path of the metallic diapir could provide a prefential low viscosity chanel for the following differentiation events.

Proposing predictive models for the thermal consequences of differentiation after an impact is fundamental in order to understand the thermal state of the interior of growing planets. As shown in Ricard et al. (2009), core formation of terrestrial protoplanets could be the consequence of a runaway segregation induced by a large enough impact on undifferentiated material. These results also underline the importance of accretionary conditions (size and temporal

repartition of impacts) on the thermal energy repartition and, hence, on the magnetic history of growing planets (Elkins-Tanton et al., 2005).

Acknowledgements

The authors thank H. Samuel and M. Jellinek for helpfull discussions. The authors also thank and H. Schmeling, T. Spohn and anonymous reviewers for constructive comments. This project was funded by the A.N.R. ETHER.

References

Agee, C. B., 1997. Melting temperatures of the Allende meteorite: implications for a Hadean magma ocean. Phys. Earth Planet. Int. 100, 41–47.

Behounkova, M., Choblet, G., 2009. Onset of convection in a basally heated spherical shell, application to planets. Earth Planet. Sci. Lett., submitted.

Christensen, U. R., Yuen, D. A., 1985. Layered convection induced by phase transitions. J. Geophys. Res. 90, 10291–10300.

Croft, S. K., 1982. A first-order estimate of shock heating and vaporization in oceanic impacts. Vol. 190. Geological Implications of Impacts of Large Asteroids and Comets on Earth, edited by T.L. Silver and P.H. Schultz,Spec. Pap. Geol. Soc. Am.

Davies, G. F., 1982. Ultimate strength of solids and formation of planetary cores. Geophys. Res. Lett. 9, 1267–1270.

Douglas, J., 1955. On the numerical integration of $\frac{\partial^2 u}{\partial x^2} + \frac{\partial^2 u}{\partial y^2} = \frac{\partial u}{\partial t}$ by implicit methods. J. Soc. Ind. Appl. Math. 3, 42–65.

Elkins-Tanton, L. T., Zaranek, S. E., Parmentier, E. M., Hess, P. C., 2005. Early magnetic field and magmatic activity on Mars from magma ocean cumulate overturn. Earth Planet. Sci. Lett. 236, 1–12.

Fei, Y., Bertka, C. M., Finger, L. W., 1997. High-Pressure Iron-Sulfur Compound, Fe3S2, and Melting Relations in the FeFeS System. Science 275, 1621–1623.

Flasar, F. M., Birch, F., 1973. Energetics of core formation: A correction. J. Geophys. Res. 78, 6101–6103.

Gerya, T. V., Yuen, D. A., 2007. Robust characteristics method for modelling multiphase visco-elastic thermo-mechanical problems. Phys. Earth Planet. Int. 163, 83–105.

Ghosh, A., McSween, H. Y., 1998. A Thermal Model for the Differentiation of Asteroid 4 Vesta, Based on Radiogenic Heating. Icarus 134, 187–206.

Golabek, G. J., Schmeling, H., Tackley, P. J., 2008. Earth's core formation aided by flow channelling instabilities induced by iron diapirs. Earth Planet. Sci. Lett. 271, 24–33.

Hadamard, J., 1911. Mouvement permanent lent d'une sphère liquide et visqueuse dans un liquide visqueux. C. R. Acad. Sci. 152, 1735–1738.

Hewitt, J. M., McKenzie, D. P., Weiss, N. O., 1975. Dissipative heating in convective flows. Journal of Fluid Mechanics 68, 721–738.

Höink, T., Schmalzl, J., Hansen, U., 2005. Formation of compositional structures by sedimentation in vigorous convection. Phys. Earth Planet. Int. 153, 11–20.

Honda, R., Mizutani, H., Yamamoto, T., 1993. Numerical simulation of Earth's core formation. J. Geophys. Res. 98, 2075–2090.

Kleine, T., Münker, C., Mezger, K., Palme, H., 2002. Rapid accretion and early core formation on asteroids and the terrestrial planets from Hf-W chronometry. Nature 418, 952–955.

Laney, C. B., 1998. Computational gasdynamics. Cambridge University Press, Cambridge.

Monteux, J., 2009. Modélisation numérique de la formation du noyau terrestre : contribution des impacts météoritiques. Ph.D. thesis, Université Claude Bernard Lyon 1.

Monteux, J., Coltice, N., Dubuffet, F., Ricard, Y., 2007. Thermo-mechanical adjustment after impacts during planetary growth. Geophys. Res. Lett. 34, 24201–24205.

O'Keefe, J. D., Ahrens, T. J., 1977. Impact-induced energy partitioning, melting, and vaporization on terrestrial planets. In: Merril, R. B. (Ed.), Lun. Planet. Sci. Conf. Vol. 8. pp. 3357–3374.

Peaceman, D. W., Rachford, H. H., 1955. The numerical solution of parabolic and elliptic differential equations. J. Soc. Ind. Appl. Math. 3, 28–41.

Pierazzo, E., Vickery, A. M., Melosh, H. J., 1997. A Reevaluation of Impact Melt Production. Icarus 127, 408–423.

Ratcliff, J. T., Tackley, P. J., Schubert, G., Zebib, A., 1997. Transitions in thermal convection with strongly variable viscosity. Phys. Earth Planet. Int. 102, 201–212.

Ribe, N. M., 2007. Analytical Methods in Mantle Dynamics, Treatise of Geophysics. Vol. 7. Schubert, G. editor in Chief, Elsevier.

Ricard, Y., 2007. Physics of Mantle Convection, Treatise of Geophysics. Vol. 7. Schubert, G. editor in Chief, Elsevier.

Ricard, Y., Sramek, O., Dubuffet, F., 2009. A multi-phase model of runaway core-mantle segregation in planetary embryos. Earth Planet. Sci. Lett., in press.

691 Roe, P. L., 1986. Characteristic-based schemes for the Euler equations. Annual
692 Review of Fluid Mechanics 18, 337–365.

693 Rybczynski, W., 1911. über die fortschreitende bewegung einer flüssigen kugel
694 in einen medium. Bull. Acad. Sci. Cracovie 1, 40–46.

695 Samuel, H., Tackley, P. J., 2008. Dynamics of core formation and equilibration
696 by negative diapirism. Geochem. Geophys. Geosyst. 9, 6011–6026.

697 Schubert, G., Turcotte, D. L., Olson, P., Sep. 2001. Mantle convection in the
698 Earth and planets. Cambridge University Press.

699 Senshu, H., Kuramoto, K., Matsui, T., 2002. Thermal evolution of a growing
700 Mars. J. Geophys. Res. 107, 1–13.

701 Shannon, M. C., Agee, C. B., 1996. High pressure constraints on percolative
702 core formation. Geophys. Res. Lett. 23, 2717–2720.

703 Sramek, O., 2007. Modèle d'écoulement biphasé en sciences de la terre: fu-
704 sion partielle, compaction et différenciation,. Ph.D. thesis, Ecole Normale
705 Supérieure de Lyon.

706 Stevenson, D. J., 1989. Formation and early evolution of the Earth. in Mantle
707 convection and plate tectonics, W.R. Peltier, ed.

708 Stevenson, D. J., 1990. Fluid dynamics of core formation. Origin of the Earth
709 edited by H. E. Newsom and J. H. Jones, eds., Oxford Univ., New York.

710 Tonks, W. B., Melosh, H. J., 1992. Core formation by giant impacts. Icarus 100,
711 326–346.

712 Touboul, M., Kleine, T., Bourdon, B., Palme, H., Wieler, R., 2007. Late forma-
713 tion and prolonged differentiation of the Moon inferred from W isotopes in
714 lunar metals. Nature 450, 1206–1209.

Vocadlo, L., Alfè, D., Price, G. D., Gillan, M. J., 2000. First principles calculations on the diffusivity and viscosity of liquid fe-s at experimentally accessible conditions. Phys. Earth Planet. Int. 120, 145–152.

Von Bargen, N., Waff, H. S., 1986. Permeabilities, interfacial areas and curvatures of partially molten systems: Results of numerical computations of equilibrium microstructures. J. Geophys. Res. 91, 9261–9276.

Yin, Q., Jacobsen, S. B., Yamashita, K., Blichert-Toft, J., Télouk, P., Albarède, F., 2002. A short timescale for terrestrial planet formation from Hf-W chronometry of meteorites. Nature 418, 949–952.

Yoshino, T., Walter, M. J., Katsura, T., 2003. Core formation in planetesimals triggered by permeable flow. Nature 422, 154–157.

Ziethe, R., Spohn, T., 2007. Two-dimensional stokes flow around a heated cylinder: A possible application for diapirs in the mantle. J. Geophys. Res. 112, 1–13.

Table 1: Typical parameter values for numerical models

Planet radius	R	1000 - 4000 km
Impactor radius	R_{imp}	100 - 400 km
Silicate density	ρ_{Si}	3500 kg m^{-3}
Iron density	ρ_{Fe}	8000 kg m^{-3}
Density difference	$\Delta\rho_0 = \rho_{Fe} - \rho_{Si}$	4500 kg m^{-3}
Average density	ρ_0	4270 kg m^{-3}
Heat capacity	$\overline{\rho C_p}$	$4{\times}10^3$ kJ K^{-1} m^{-3}
Heat diffusivity	κ	10^{-6} m^2 s^{-1}
Thermal conducivity	k	4 W m^{-1} K^{-1}
Initial temperature	T_0	K
Metal content	f_0	0.17
Viscosity	η_0	10^{22} Pa s
Viscosity factor	λ	$2.5 \times 10^{-2} - 1$
Gravity	$g_0 = 4\pi G\rho_0 R/3$	m s^{-2}
Stokes velocity scale	$\Delta\rho_0 g_0 R^2/\eta_0$	$\sim$100 m/yr
Time scale	$\eta_0/\Delta\rho_0 g_0 R$	$\sim$20 kyr
Rayleigh number Ra_χ	$\overline{\rho C_p}\Delta\rho_0 g_0 R^3/\eta_0 k$	$\sim 10^8$
Buoyancy B	$\Delta\rho_0/\alpha\rho_0\Delta T_0$	25-250
Dissipation number D_χ	$\Delta\rho_0 g_0 R/\overline{\rho C_p}\Delta T_0$	36.6
Impact energy conversion coefficient	γ	0.3
Volume effectively heated by impact	$h(m)$	2.7
Stokes velocity coefficient	c_1	0.1-0.2
Heat diffusion coefficient	c_2	0.3-1.05

Table 2: Values obtained fitting numerical experiments with theoretical predictions (Eq.12 and Eq.30) for different values of λ (with $R = 2000$ km and $R_{imp} = 300$ km)

	$\lambda = 1$	$\lambda = 0.25$	$\lambda = 0.1$	$\lambda = 2.5 \times 10^{-2}$
τ_S	563	249	170	114
τ_D	20 054	16 520	13 316	8974
a	19%	14.7%	11%	7%

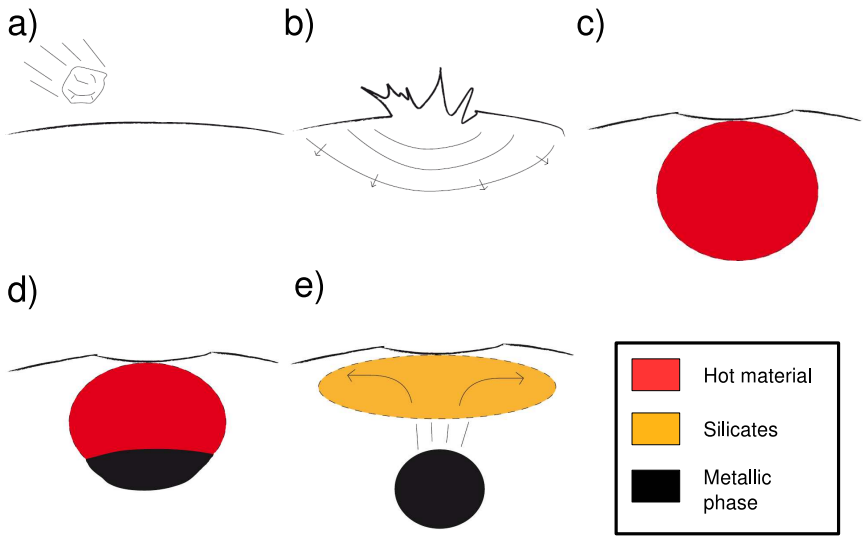

Figure 1: Schematic view of the chemical equilibration following a large impact on an undifferentiated protoplanet. In the isobaric core resulting from the dissipation of the shock wave (a,b), the temperature increase (c) melts the metal that segregates rapidly (d), then sinks toward the planetary embryo center by a diapiric instability (e).

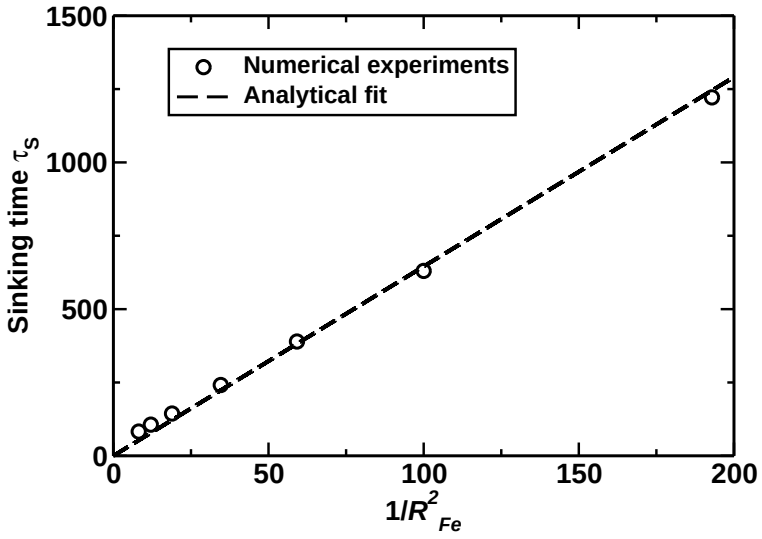

Figure 2: Characteristic sinking time τ_S as a function of $1/R^{*2}_{Fe}$, where R^*_{Fe} is the non-dimensionalized metallic sphere radius. Results from numerical experiments (with uniform viscosity $\eta_S = 10^{22}$ and $R = 1000$ km) are representated with black circles. Theoretical fit from Eq.13 is shown by the dashed line with $c_1 = 0.187$.

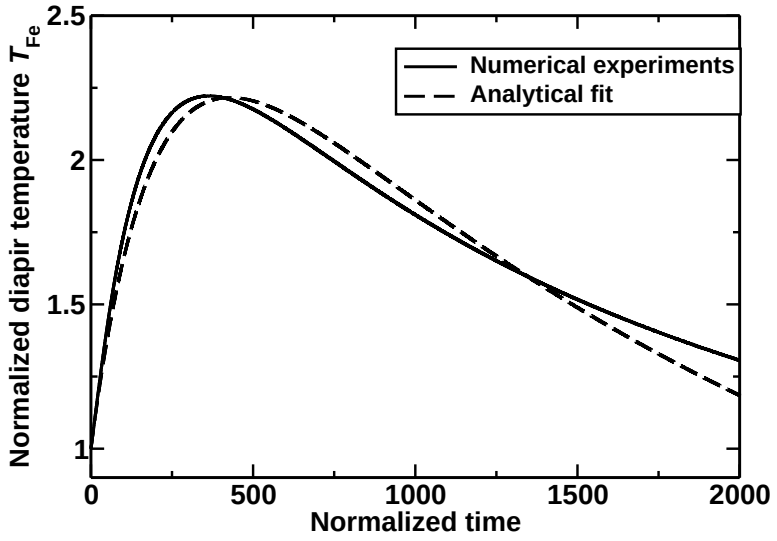

Figure 3: Temperature evolution (black line) of a metallic sphere ($R_{Fe} = 130$ km) falling in an undifferentiated planet with $R = 1000$ km. Theoretical evolution from Eq.30 is shown with a dashed line ($c_1 = 0.187$, $c_2 = 0.72$ and $a = 20\%$).

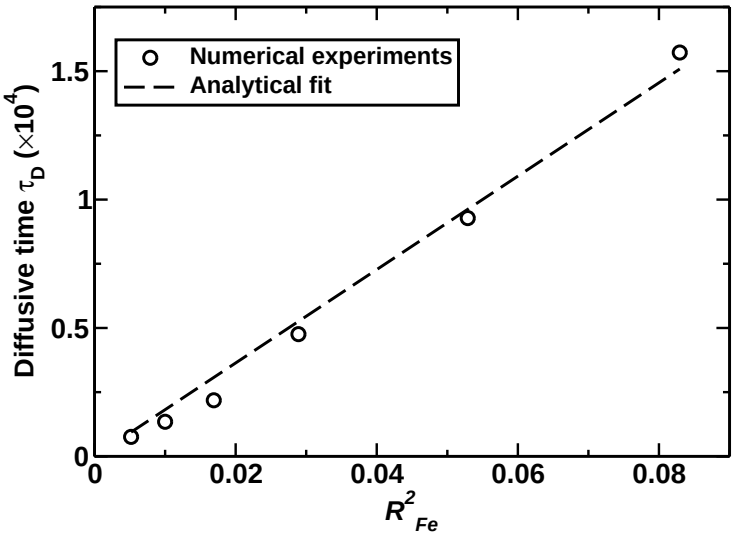

Figure 4: Non-dimensional characteristic time of diffusion τ_D as a function of the non-dimensionalized metallic sphere radius. Results from numerical experiments (with a uniform viscosity and $R = 1000$ km) are represented with black circles. Theoretical fit from Eq.26 is shown in dashed line with $c_2 = 1.01$.

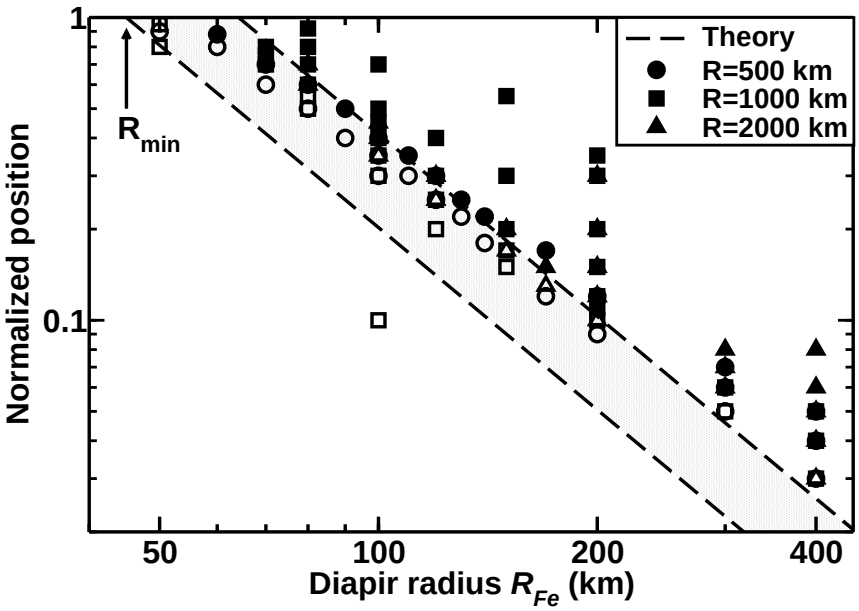

Figure 5: Thermal behaviour of a sinking metal sphere in an undifferentiated media as function of position and sphere radius. Each symbol represents the instantaneous thermal behaviour of an hot metallic sphere with radius R_{Fe} for a given initial position. Filled symbols represent numerical experiments with viscous heating and open symbols represent numerical experiments with only cooling. Different symbols characterize different planets radii. The analytical transition between heating and cooling is predicted within the shaded area and the boarders of this area are defined with $\Delta T_{max}/\Delta T_0$ between 1 (no heating) and 4.2 (maximum heating)(see, Eq.32).

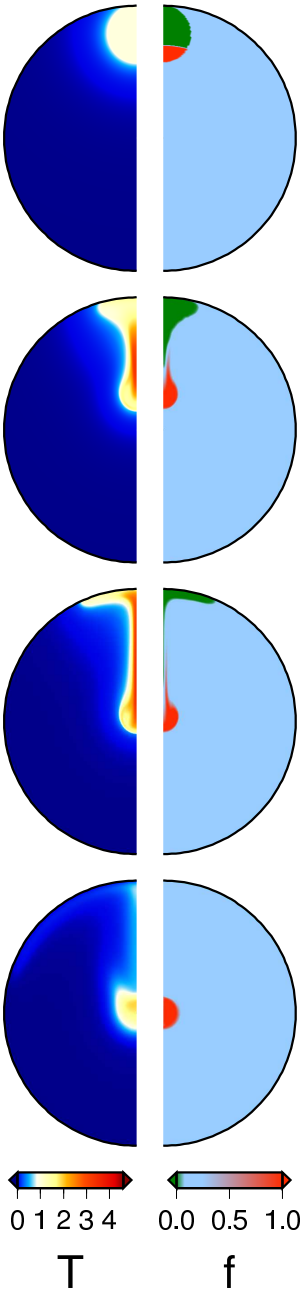

Figure 6: Non dimensional temperature (left) and composition (right) at times $t = 0$ (first line), $t = 1.4$ My (second line), $t = 3.8$ My (third line) and $t = 546$ My (fourth line) (computed for a uniform viscosity with $R = 4000$ km, $R_{imp} = 600$ km and 200×200 grid points)

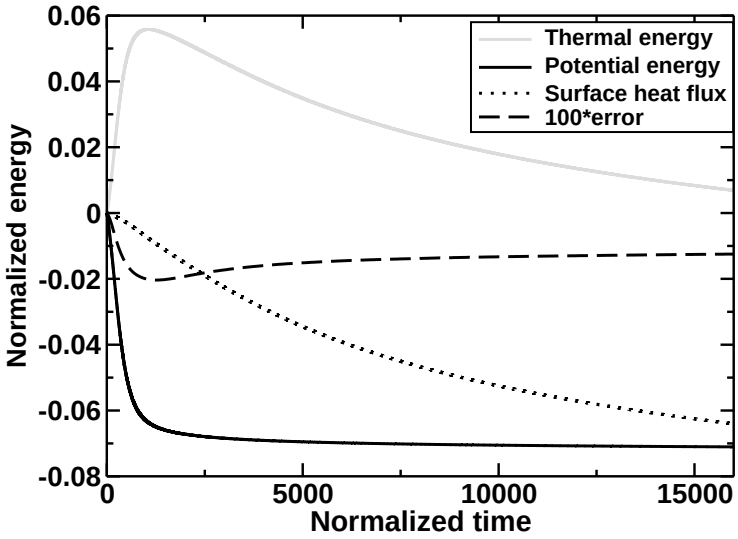

Figure 7: Non dimensionalized potential (solid black line) and thermal (solid grey line) energies and time integrated surface heat flow (dotted black line) as functions of time. The sum of these three quantities times 100 is shown in dashed black line. Its difference to zero is indicative of the accuracy of the energy conservation of the numerical code (for $R = 2000$ km, $R_{imp} = 300$ km and $R_{Fe} = 240$ km and uniform viscosity).

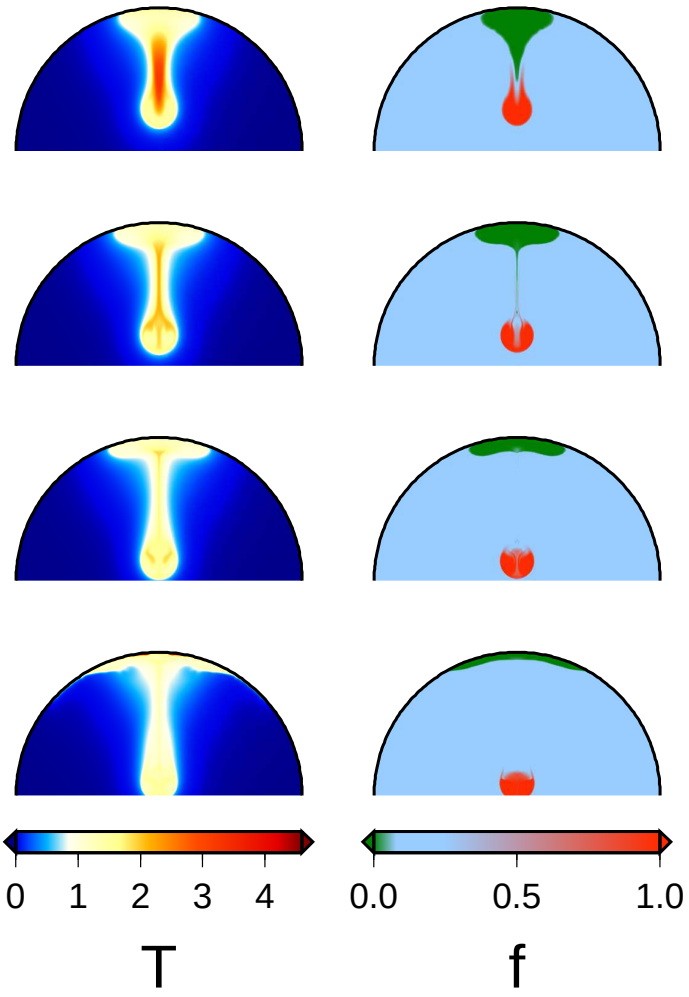

Figure 8: The four rows depict the temperature (left) and the composition (right) at $t = 3.2$ My (with $R = 2000$ km and $R_{imp} = 300$ km), for a uniform viscosity (top) and for variable viscosities (contrast of ~ 16 (second row), ~ 100 (third row) and ~ 1600 (bottom row)). As expected, the sinking velocity of the metallic diapir and the rising velocity of the silicates, both increase when their viscosity is decreased.

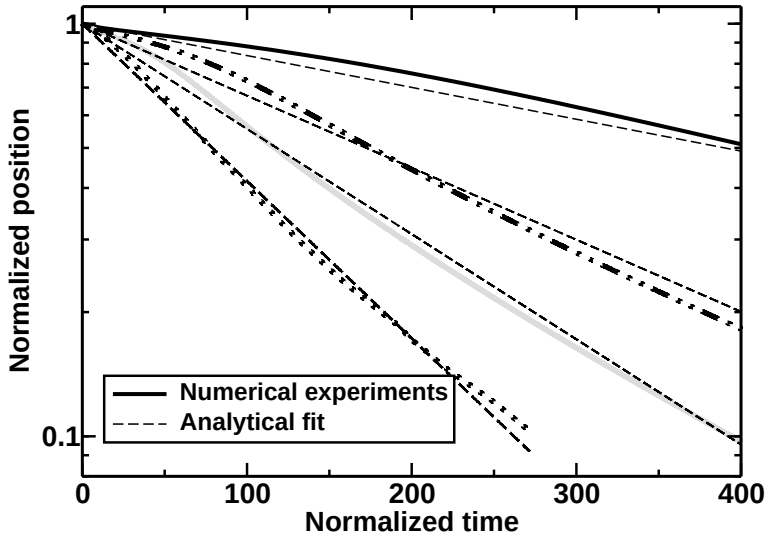

Figure 9: Position of the inertia center of the metal phase as a function of time for a uniform viscosity (black line) and for temperature-dependent viscosities with $\lambda = 0.25$ (dashed dotted line), $\lambda = 0.1$ (grey line) and $\lambda = 2.5 \times 10^{-2}$ (dotted line) ($R = 2000$ km and $R_{imp} = 300$ km). Thin dashed lines correspond to simple exponential fittings from which the sinking times are extracted (see Tab.2).

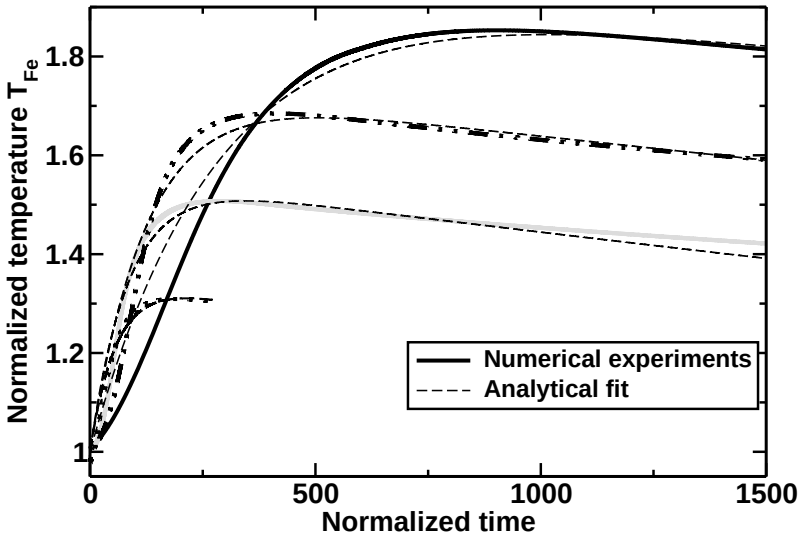

Figure 10: Temperature evolution of the metal phase as a function of time for a uniform viscosity (solid black line) and for temperature-dependent viscosities with $\lambda = 0.25$ (dashed dotted line), $\lambda = 0.1$ (grey line) and $\lambda = 2.5 \times 10^{-2}$ (dotted line) ($R = 2000$ km and $R_{imp} = 300$ km). Thin dashed lines correspond to theoretical results from Eq.30 from which the diffusive times and the proportion of energy heating the metal diapir are extracted (see Tab.2).